*Int. J. Appl. Math. Comput. Sci., 2026, Vol. 36, No. 3, 433–444*
DOI: 10.61822/amcs-2026-0028

# A FIXED–TIME POSITIONAL PATH–FOLLOWING CONTROL SYSTEM FOR UNICYCLE–LIKE MOBILE ROBOTS WITH CONSTRAINED INPUTS: DESIGN AND ROBUSTNESS

MACIEJ MARCIN MICHAŁEK [a,*], MIKOŁAJ JERZY PRZYBYLSKI [a]

[a] Institute of Automatic Control and Robotics
Poznan University of Technology
Piotrowo 3A, 61-138 Poznań, Poland
e-mail: maciej.michalek@put.poznan.pl

This paper presents a fixed-time solution to the positional path-following control task for unicycle-like mobile robots with constraints imposed on the control inputs. The proposed control system, designed for a guidance point located out of the robot wheels' axle, guarantees local convergence of a positional error for a guidance point in finite time which is upper bounded by a constant (independent of an initial robot configuration). Apart from control derivation and a stability proof conducted for closed-loop dynamics, the paper includes also a robustness analysis which reveals how the fixed-time control function improves robustness of the closed-loop system to external perturbations affecting the control input channels of a robot. Numerical simulations and experimental results validate the concept, and also highlight some computational and implementation issues important in practical applications.

**Keywords:** intelligent systems, fixed-time control, path following, nonholonomic unicycle-like mobile robot, constrained control inputs, robustness.

## 1. Introduction

Path following belongs today to the most popular tasks considered for mobile robots and automated vehicles in practical applications. Literature devoted to automated execution of this task is very rich (see, e.g., de Wit *et al*., 1996; Lapierre *et al*., 2006; Morin and Samson, 2008; Mazur and Szakiel, 2009; Mazur and Dyba, 2025). In a classical approach, a reference path is defined as a curvilinearly parametrized line, while more recent approaches use a reference path represented as a set of points belonging to the cross-section of a two-argument function and a zero-level plane (Consolini *et al*., 2010; Morro *et al*., 2011; Michałek and Gawron, 2018; Yao *et al*., 2021; Yao *et al*., 2023).

Most of the feedback control functions developed to solve the problem of automated path following lead to asymptotic convergence of the error in an infinite time horizon (Płaskonka, 2015). However, in applications where a time-synchronized motion plays a crucial role (like multi-vehicle formation making, one-shot docking maneuvers, sequencial motion tasks, or other safety-critical maneuvers), a control system should guarantee convergence of the error in *fixed time*, where a maximal upper bound imposed on a settling time is guaranteed independently of an initial condition (in contrast to *finite-time* control (Moulay and Perruquetti, 2006; Efimov and Polyakov, 2021)). This type of convergence can be ensured by the so-called fixed-time control, which has been proposed in numerous publications since the beginning of the current century (see, e.g., Bhat and Bernstein, 2000), but more deeply investigated recently (e.g., Polyakov, 2012; Aldana-Lopez *et al*., 2019).

One can find numerous applications of the fixed-time control idea to dynamical systems, including nonholonomic ones (cf. Zhang *et al*., 2019; Sanchez-Torres *et al*., 2020; Lin *et al*., 2021; Dai *et al*., 2021; Garg *et al*., 2022; Gao *et al*., 2022; Ou *et al*., 2022; Zhou *et al*., 2025; Sobański *et al*., 2025). Despite the applications mentioned, there still remains a room for fixed-time control applications in constrained robotics. Therefore, in the current paper, we

*Corresponding author

try to fill a gap of the literature devoted to applications of fixed-time control to nonholonomic mobile robots. Namely, we propose a fixed-time control law for unicycle-like nonholonomic kinematics with constrained control inputs to solve the positional path-following control task, where the guidance point of a robot is located out of the wheels' axle (de Wit *et al.*, 1996), and a reference path is determined by a zero-level set of a position-dependent function (Morro *et al.*, 2011; Consolini *et al.*, 2010; Yao *et al.*, 2021; 2023). In the paper, we also show how the fixed-time controller can improve robustness of closed-loop dynamics to velocity perturbations, relative to the non-fixed-time solutions. In our approach, a reference path is represented as a zero-level curve of a positionally-evaluated function. A control law explicitly takes into account control inputs constraints imposed on (velocity) control signals of a mobile robot. Moreover, we provide a robustness analysis of closed-loop dynamics in relation to external perturbations affecting the control signals.

This paper is a substantial extension of the preliminary conference work presented by Michałek *et al.* (2025). The new results include incorporation of control inputs constraints of a mobile robot, a modified robustness analysis for closed-loop dynamics, a more detailed numerical study, and an experimental validation of the proposed control approach with a laboratory-scale mobile robot.

**Notation.** Throughhout the paper, $\|\cdot\|$ denotes the 2-norm of a vector or an induced 2-norm of a matrix, $\triangleq$ stands for equality *by definition*, for a scalar argument $a$ we write $\lfloor a \rceil^{\eta} \triangleq \operatorname{sign}(a)\,|a|^{\eta}$ and $\frac{\mathrm{d}\lfloor a \rceil^{\eta}}{\mathrm{d}a} = \eta\,|a|^{\eta-1}$, $\dot{a} \equiv \mathrm{d}a/\mathrm{d}t$, and the function $\operatorname{sign}(a)$ is zero at $a = 0$.

## 2. Prerequisites and the control problem

**2.1. Fixed-time stability: Recalling the main results.** In order to make the subsequent formal considerations strict enough, we recall here the main results on fixed-time stability. Let us consider a dynamical system $S$: $\dot{\boldsymbol{z}}(t) = \boldsymbol{f}(\boldsymbol{z}(t))$ and its trajectory $\boldsymbol{z}(t, \boldsymbol{z}_0) \in \mathbb{R}^n$, defined for $t \geq 0$ and starting from an initial condition $\boldsymbol{z}_0 \triangleq \boldsymbol{z}(t = 0)$. Moreover, we assume that the constant trajectory $\boldsymbol{z}(t, \boldsymbol{0}) \equiv \boldsymbol{0}$ is an equilibrium point of system $S$, that is, $\boldsymbol{f}(\boldsymbol{0}) \equiv \boldsymbol{0}$. Following, e.g., Polyakov (2012), Aldana-Lopez *et al.* (2019) or Sobański *et al.* (2025), let us formulate the following key definition and lemma.

**Definition 1.** (*Fixed-time stability*) An equilibrium point $\boldsymbol{z} = \boldsymbol{0}$ of system $S$ is called fixed-time stable if it is stable in the sense of Lyapunov, and additionally $\boldsymbol{z}(t, \boldsymbol{z}_0) = \boldsymbol{0}$ for all $t \geq t_s(\boldsymbol{z}_0)$ where $t_s(\boldsymbol{z}_0) < \infty$ is called the settling time, and there exists an upper bound $T_s < \infty$ such that $t_s(\boldsymbol{z}_0) \leq T_s$ for any initial condition $\boldsymbol{z}_0 \in \mathbb{R}^n$.

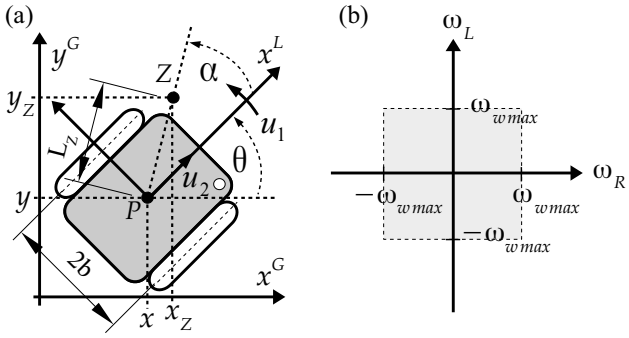



Fig. 1. Kinematics of the unicycle-like mobile robot with a definition of point $Z$ (a), a set of the admissible robot's wheel speeds which determines the constrained set $\mathcal{U}$ of the robot's control inputs (b).

**Lemma 1.** *An equilibrium point $\boldsymbol{z} = \boldsymbol{0}$ of system $S$ is fixed-time stable in a domain $\mathcal{D}_z \subseteq \mathbb{R}^n$ if there exists a positive-definite radially unbounded continuous function $V(\boldsymbol{z}) : \mathcal{D}_z \to \mathbb{R}_+ \cup \{0\}$ such that any trajectory $\boldsymbol{z}(t, \boldsymbol{z}_0)$ of system $S$, starting from an initial condition $\boldsymbol{z}_0 \in \mathcal{D}_z$, satisfies*

$$\dot{V}(\boldsymbol{z}(t, \boldsymbol{z}_0)) \leq -\gamma_1 V^{p_1}(\boldsymbol{z}(t, \boldsymbol{z}_0)) - \gamma_2 V^{p_2}(\boldsymbol{z}(t, \boldsymbol{z}_0)) \quad (1)$$

*for $t \geq 0$ and $\gamma_1, \gamma_2 > 0$, $p_1 > 1$, $p_2 \in (0; 1)$.*

**2.2. Kinematics of unicycle-like mobile robots.** Let us consider kinematics of a unicycle-like mobile robot:

$$\dot{\boldsymbol{q}} = \begin{bmatrix} \dot{\theta} \\ \dot{x} \\ \dot{y} \end{bmatrix} = \begin{bmatrix} 1 & 0 \\ 0 & \cos\theta \\ 0 & \sin\theta \end{bmatrix} \begin{bmatrix} u_1 \\ u_2 \end{bmatrix} = \boldsymbol{G}(\boldsymbol{q})\boldsymbol{u}, \quad (2)$$

where the configuration vector $\boldsymbol{q} \triangleq [\theta\ x\ y]^{\top} \in \mathbb{R}^3$ comprises an orientation angle $\theta$ of the robot's body in a global frame and coordinates $x, y$ of the mid-point $P$ located between the wheels. The control vector $\boldsymbol{u} \in \mathcal{U} \subset \mathbb{R}^2$ contains the angular robot speed $u_1$ of a robot's platform and the longitudinal speed $u_2$ of the point $P$, whereas $\mathcal{U}$ represents a compact subset of $\mathbb{R}^2$ (a set of control constraints) where the control signals, $u_1(t)$ and $u_2(t)$, must stay in the whole control time-horizon.

We complement the kinematics (2) with an output equation:

$$\boldsymbol{y}(\boldsymbol{q}) = \begin{bmatrix} y_1(\boldsymbol{q}) \\ y_2(\boldsymbol{q}) \end{bmatrix} \triangleq \begin{bmatrix} x + L_Z\cos(\theta + \alpha) \\ y + L_Z\sin(\theta + \alpha) \end{bmatrix} \in \mathbb{R}^2, \quad (3)$$

which determines the position of point $Z = (x_Z, y_Z)$ (cf. Fig. 1), which will be treated as the *guidance point* for a positional control task defined in the sequel. The location of guidance point $Z$ is determined by two constant parameters: a distance $L_Z > 0$ and an angle $\alpha \in (-\pi; \pi]$,

$|\alpha| \neq \pi/2$, both selected by a user. It is well known (see de Wit *et al.*, 1996) that selection of the output (3) under the mentioned limitations imposed on parameters $L_Z$ and $\alpha$ enables application of a feedback-linearization idea, which will be used in Section 3.1.

**2.3. Input signals limitations: Velocity scaling.** In order to address the limitations imposed on the robots' control inputs, let us recall the following velocity scaling procedure (see, e.g., Oriolo *et al.*, 2002; Michałek and Gawron, 2018). First, assume that $\boldsymbol{\phi} = [\phi_1 \ \phi_2]^\top \in \mathbb{R}^2$ represents here an original (nominal) control function defined for unicycle kinematics without considering any control inputs limitations. The control signals satisfying the constrained set $\mathcal{U}$ can be computed as follows:

$$\boldsymbol{u}(t) = s(t)\boldsymbol{\phi}(t) \quad \Rightarrow \quad \boldsymbol{u}(t) \in \mathcal{U} \quad \forall\, t \geq 0, \tag{4}$$

with the scaling function

$$s(t) \triangleq \left[\max\left\{1, \frac{|\omega_{Rc}(t)|}{\omega_{w\max}}, \frac{|\omega_{Lc}(t)|}{\omega_{w\max}}\right\}\right]^{-1} \in (0;1], \tag{5}$$

where $\omega_{w\max} > 0$ is a maximal admissible angular speed of a robot's wheel, $[\omega_{Rc}\, \omega_{Lc}]^\top = \boldsymbol{J}^{-1}\boldsymbol{\phi}$, whereas $\boldsymbol{J}^{-1} = \begin{bmatrix} b/r & 1/r \\ -b/r & 1/r \end{bmatrix}$ is an inverted Jacobian matrix dependent on the wheel's radius $r > 0$ and a half distance $b > 0$ between the robot's wheels (cf. Fig. 1). The terms $\omega_{Rc}(t)$ and $\omega_{Lc}(t)$ represent the instantaneous desired angular speeds computed for the robot's wheels which correspond to the instantaneous nominal speeds $\phi_1(t)$ and $\phi_2(t)$ of a robot platform obtained by the function $\boldsymbol{\phi}$. It is evident that application of the scaling procedure (4) into the driftless dynamics (2) preserves the original curvature of a robot motion determined by $\kappa(t) = \phi_1(t)/\phi_2(t)$.

**2.4. Non-parametrized positional reference path.** A reference path will be defined as a zero-level set of a function $F(\boldsymbol{y})$, well defined on a compact positional set $\mathcal{D} \subset \mathbb{R}^2$. Namely, the reference path will be represented as the set (Michałek and Gawron, 2018)

$$S_d \triangleq \{\boldsymbol{y}_d \in \mathcal{D} :\ F(\boldsymbol{y} = \boldsymbol{y}_d) = 0\}, \tag{6}$$

where $F(\boldsymbol{y}_d) \triangleq \sigma f(\boldsymbol{y}_d) = 0$ denotes a zero-level set of function $F(\boldsymbol{y})$ whereas $\sigma \in \mathbb{R} \setminus \{0\}$ is a design scaling factor. The sign of $\sigma$ determines a desired reference motion strategy along the path (i.e., left-right or clockwise-counterclockwise), while its absolute value affects the gradient of function $F(\boldsymbol{y})$. A particular form of function $F(\boldsymbol{y})$ determines the shape of the reference path in the workspace of a robot. From now on, we will assume what follows (cf. Morro *et al.*, 2011; Michałek and Gawron, 2018):

*A1.* $F(\boldsymbol{y})$ is bounded in domain $\mathcal{D}$, that is, $\forall \boldsymbol{y} \in \mathcal{D}$ holds $F(\boldsymbol{y}) \in [\underline{F}; \overline{F}] \subset \mathbb{R}$, where $\underline{F} \in (-\infty; 0), \overline{F} \in (0; \infty)$;

*A2.* $F(\boldsymbol{y})$ is differentiable in domain $\mathcal{D}$ with respect to both arguments, that is, there exist derivatives

$$F_i(\boldsymbol{y}) \triangleq \frac{\partial F(\boldsymbol{y})}{\partial y_i}, \quad i \in \{1, 2\}, \tag{7}$$

such that, for all $\boldsymbol{y} \in \mathcal{D}$,

$$\| \nabla \boldsymbol{F}(\boldsymbol{y})\| \in [g; G], \quad \nabla \boldsymbol{F}(\boldsymbol{y}) \triangleq \begin{bmatrix} F_1(\boldsymbol{y}) \\ F_2(\boldsymbol{y}) \end{bmatrix}, \tag{8}$$

where $0 < g < G < \infty$ are the lower and upper bounds of the norm of gradient $\nabla \boldsymbol{F}$. Upon the assumption (8), a versor of a negative gradient of function $F(\boldsymbol{y})$,

$$\boldsymbol{\vartheta}(\boldsymbol{y}) \triangleq \frac{-\nabla \boldsymbol{F}(\boldsymbol{y})}{\| \nabla \boldsymbol{F}(\boldsymbol{y})\|} = \begin{bmatrix} -F_1(\boldsymbol{y}) / \| \nabla \boldsymbol{F}(\boldsymbol{y})\| \\ -F_2(\boldsymbol{y}) / \| \nabla \boldsymbol{F}(\boldsymbol{y})\| \end{bmatrix}, \tag{9}$$

is well determined in the whole domain $\mathcal{D}$.

In view of the definition (6), the value of function $F(\boldsymbol{y})$ evaluated at the current position $\boldsymbol{y}$ of point $Z$ (cf. (3)) can be treated as a measure of a positional error for the path-following task under consideration. Thus, a control problem under consideration will be defined in the next subsection with respect to function $F(\boldsymbol{y})$.

**2.5. Positional fixed-time path-following problem.** We are interested in finding a feedback control function $\boldsymbol{u} = \boldsymbol{u}(\boldsymbol{q})$ for the kinematics (2) which guarantees that in the obstacle-free positional workspace $\mathcal{D} \subset \mathbb{R}^2$, for any initial condition $\boldsymbol{y}_0 \triangleq \boldsymbol{y}(t = 0) \in \mathcal{D}$, the following relationships hold:

*R1.* $\forall t \geq 0 \quad |F(\boldsymbol{y}(t))| < \infty$,

*R2.* $\forall t \geq 0 \quad \boldsymbol{u}(\boldsymbol{q}(t)) \in \mathcal{U}$,

*R3.* $\exists\, t_s(\boldsymbol{y}_0) : \forall t \geq t_s(\boldsymbol{y}_0) \quad F(\boldsymbol{y}(t)) = 0$,

*R4.* $\sup_{\boldsymbol{y}_0 \in \mathcal{D}} t_s(\boldsymbol{y}_0) = T_s < \infty$,

where $t_s(\boldsymbol{y}_0)$ denotes the settling time of function $F(\boldsymbol{y}(t))$ achieved for the initial position $\boldsymbol{y}_0$, whereas $T_s$ is an upper bound of the settling time, independent of $\boldsymbol{y}_0$.

R1 to R2 require, respectively, a boundedness of the positional error (represented by $F(\boldsymbol{y})$) and satisfaction of the inputs constraints by the control function within the whole time-horizon of a control process. R3 imposes convergence of the positional error in finite time, while R4 requires that the maximal settling/convergence time for all the initial positions in the subset $\mathcal{D}$ must not be longer than the finite constant $T_s$.

## 3. Control law design and stability analysis

**3.1. Formulation of the fixed-time controller.** In order to define a control law for the fixed-time positional path-following problem, let us recall first the well-known dynamics of the positional output (3) with respect to the control inputs of the kinematics (2). They result from the following equation (see, e.g., de Wit *et al*., 1996):

$$\dot{\boldsymbol{y}} = \begin{bmatrix} \dot{y}_1 \\ \dot{y}_2 \end{bmatrix} = \underbrace{\begin{bmatrix} -L_Z \sin(\theta+\alpha) & \cos\theta \\ L_Z \cos(\theta+\alpha) & \sin\theta \end{bmatrix}}_{\boldsymbol{D}(\theta)} \boldsymbol{u}. \tag{10}$$

Note that matrix $\boldsymbol{D}(\theta)$ is non-singular if $\det \boldsymbol{D}(\theta) = -L_Z \cos\alpha \neq 0$, which justifies the constraints imposed on the values of parameters $L_Z$ and $\alpha$ introduced below the definition (3). Satisfying these constraints, the matrix $\boldsymbol{D}(\theta)$ is invertible for any orientation angle $\theta$. Substitution into (10) of the scaled feedback-linearization control law

$$\boldsymbol{u} \triangleq s\boldsymbol{\phi}, \qquad \boldsymbol{\phi} \triangleq \boldsymbol{D}^{-1}(\theta)\boldsymbol{w}, \tag{11}$$

with the scaling function determined in (5) and with a new (outer-loop) control input $\boldsymbol{w} \in \mathbb{R}^2$, leads to the scaled decoupled linear dynamics

$$\dot{\boldsymbol{y}} = s\boldsymbol{w}. \tag{12}$$

Now, following the general result provided by Yao *et al*. (2021), let us define the outer-loop control function as follows (cf. also Michałek and Gawron, 2018):

$$\boldsymbol{w} \triangleq k_p h(F(\boldsymbol{y}))\boldsymbol{\vartheta}(\boldsymbol{y}) + v_d \boldsymbol{R}\boldsymbol{\vartheta}(\boldsymbol{y}), \tag{13}$$

where $v_d \in (0;\infty)$ is a constant reference longitudinal speed, $\boldsymbol{\vartheta}(\boldsymbol{y})$ was introduced in (9), $k_p > 0$ is a design coefficient, $\boldsymbol{R} = \left[\begin{smallmatrix} 0 & 1 \\ -1 & 0 \end{smallmatrix}\right]$ is a rotation matrix of angle $-\pi/2$, while

$$h(F(\boldsymbol{y})) \triangleq \lfloor F(\boldsymbol{y}) \rceil^{1+\delta} + \lfloor F(\boldsymbol{y}) \rceil^{1-\delta}, \ \delta \in (0;1), \tag{14}$$

is a feedback term defined for a parameter $\delta$ selected by the designer. It is worth noting that the second term in (14) is non-Lipschitz with respect to $F(\boldsymbol{y})$, which is crucial for achieving fixed-time convergence. Additionally, the first component in (13) is responsible for attracting point $Z$ toward a reference path, whereas the second term in (13) plays the role of feedforward control along the path. Note that the two terms are perpendicular to each other by definition. As a consequence, the control vector (13) cannot degenerate to zero in the whole domain $\mathcal{D}$. A block scheme illustrating the proposed positional control system is presented in Fig. 2.

**Remark 1.** To make a motion of point $Z$ with a reference speed $v_d$ possible, the factor $v_d$ introduced in (13) should satisfy the limitations imposed on the robot's speeds. Hence, in the perfect path-following conditions, that is, for $F(\boldsymbol{y}(t)) \equiv 0$, the velocity scaling procedure should lead to $s(t) \equiv 1$. In these conditions, one obtains (see (11)–(13)) $\boldsymbol{u} \equiv \boldsymbol{\phi} = \boldsymbol{D}^{-1}(\theta)\boldsymbol{w}$ and $\dot{\boldsymbol{y}} = \boldsymbol{w} = v_d \left[\begin{smallmatrix} \cos\gamma(\boldsymbol{y}) \\ \sin\gamma(\boldsymbol{y}) \end{smallmatrix}\right]$, where $\left[\begin{smallmatrix} \cos\gamma(\boldsymbol{y}) \\ \sin\gamma(\boldsymbol{y}) \end{smallmatrix}\right] = \boldsymbol{R}\boldsymbol{\vartheta}(\boldsymbol{y})$ is a unit vector. Recalling now the relationships from Section 2.3, one can write

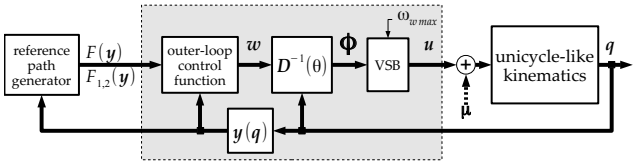



Fig. 2. Block scheme of the proposed positional control system for the unicycle-like kinematics (VSB: velocity scaling block; see the formulas (4)–(5)).

$$\begin{aligned} \left[\begin{smallmatrix} \omega_{Rc} \\ \omega_{Lc} \end{smallmatrix}\right] &= v_d \boldsymbol{J}^{-1}\boldsymbol{D}^{-1}(\theta)\boldsymbol{R}\boldsymbol{\vartheta}(\boldsymbol{y}) \\ &= v_d \begin{bmatrix} c_1 \sin(\gamma-\theta) + c_2 \cos(\gamma-\theta-\alpha) \\ -c_1 \sin(\gamma-\theta) + c_2 \cos(\gamma-\theta-\alpha) \end{bmatrix}, \end{aligned} \tag{15}$$

where $c_1 = b/(rL_Z \cos\alpha)$ and $c_2 = 1/(r\cos\alpha)$ are constants. In order to satisfy the speed limitations, that is, $|\omega_{Rc}(t)| \leq \omega_{w\max}$ and $|\omega_{Lc}(t)| \leq \omega_{w\max}$ for all $t \geq 0$, it is not difficult to check upon (15) that it leads to the following (conservative but operational) limitation of the reference speed selection:

$$v_d < \frac{rL_Z\,|\cos\alpha|}{b + L_Z}\omega_{w\max}. \tag{16}$$

We have intentionally used the acute inequality in (16) to ensure some excess in the robot's available speeds during following a path, which can be used for preserving robustness of motion control in case of possible speed perturbations affecting the robot's motion.

**3.2. Main result and stability analysis.** The main result will be presented by the following.

**Theorem 1.** *The feedback control law defined by (11) and (13)–(14) applied into the kinematics (2) solves the fixed-time path-following problem by satisfying R1 to R4.*

*Proof.* First, let us consider dynamics of the positional-error $F(\boldsymbol{y}(t))$ (we will omit the arguments for compactness of notation):

$$\begin{aligned} \dot{F} &= \nabla\boldsymbol{F}^\top \dot{\boldsymbol{y}} \overset{(10)}{=} \nabla\boldsymbol{F}^\top \boldsymbol{D}(\theta)\boldsymbol{u} \overset{(11)}{=} s\nabla\boldsymbol{F}^\top \boldsymbol{w} \\ &\overset{(13)}{=} s\nabla\boldsymbol{F}^\top k_p \left[\lfloor F \rceil^{1+\delta} + \lfloor F \rceil^{1-\delta}\right]\boldsymbol{\vartheta} + sv_d \nabla\boldsymbol{F}^\top \boldsymbol{R}\boldsymbol{\vartheta} \\ &\overset{(9)}{=} -sk_p \left[\lfloor F \rceil^{1+\delta} + \lfloor F \rceil^{1-\delta}\right] \frac{\nabla\boldsymbol{F}^\top \nabla\boldsymbol{F}}{\|\nabla\boldsymbol{F}\|} \\ &= -sk_p \|\nabla\boldsymbol{F}\| \left[\lfloor F \rceil^{1+\delta} + \lfloor F \rceil^{1-\delta}\right], \end{aligned} \tag{17}$$

where we used the fact that $\nabla \boldsymbol{F}^\top \boldsymbol{R}\vartheta \equiv 0$ due to the skew-symmetry of matrix $\boldsymbol{R}$ and the definition (9). Upon Eqn. (17), and according to the properties of the scaling function introduced in (5), it is clear that $F = 0$ is an equilibrium of positional error dynamics. Now, let us introduce a positive definite function $V(F) \triangleq F^2$. Its time derivative along solutions of the dynamics (17) can be assessed as follows (omitting the arguments):

$$\begin{aligned}\dot{V} = 2F\dot{F} &\overset{(17)}{=} -2sk_p \,\|\nabla \boldsymbol{F}\| \left[|F|^{2+\delta} + |F|^{2-\delta}\right] \\ &= -2sk_p \,\|\nabla \boldsymbol{F}\| \left[V^{(2+\delta)/2} + V^{(2-\delta)/2}\right] \\ &\leq -2gk_p\underline{s} \left[V^{1+\delta/2} + V^{1-\delta/2}\right], \end{aligned} \tag{18}$$

where in the last line we used (8) from the assumption A2, and $\underline{s} = \inf_{t\geq 0} s(t) > 0$. By recalling Lemma 1 and comparing (18) with (1), one concludes that $F(\boldsymbol{y}(t)) = 0$ is fixed-time stable in domain $\mathcal{D} \subset \mathbb{R}^2$, where $\gamma_1 = \gamma_2 = 2gk_p\underline{s} > 0$, and if $\delta \in (0;1)$ then $p_1 = (1 + \delta/2) > 1$ and $p_2 = (1 - \delta/2) \in (0;1)$. As a consequence, and by recalling Definition 1, the relationships R1, R3, and R4 are satisfied in domain $\mathcal{D}$. It is evident that, by invertability of matrix $\boldsymbol{D}(\theta)$, by the definition (13), thanks to the scaling procedure (4), and under the assumptions A1–A2, the relation R2 holds in domain $\mathcal{D}$ as well. ■

**Remark 2.** By referring to Parsegov *et al*. (2012), one can compute the upper bound $T_s$ of a settling time $t_s(\boldsymbol{y}_0)$ (cf. Definition 1 and R4) for all initial conditions from the admissible domain $\mathcal{D}$ as $T_s = \arctan(F_m^\delta)/(gk_p\delta\underline{s})$, where $F_m = \sup_{\boldsymbol{y}_0\in\mathcal{D}} |F(\boldsymbol{y}_0)| \leq \overline{F}$ (cf. the assumption A1). Note that, due to the conservative assessment conducted in (18), the upper bound $T_s$ computed in the above manner is usually (very) conservative. Moreover, since the value $\underline{s}$ is unknown a priori (we cannot predict the infimum of $s(t)$ before a robot's motion), the upper bound $T_s$ can be only reconstructed a posteriori, i.e., after completion of a task by the robot.

## 4. Analysis of robustness to perturbations

We are interested in how the fixed-time stability influences robustness of closed-loop dynamics to a selected type of perturbations. We consider a *matched* input perturbation in the form of a vector of bounded external perturbing speeds, $\boldsymbol{\mu} = [\mu_1\ \mu_2]^\top \in \mathbb{R}^2$, directly affecting the control input channels of a mobile robot (cf. Fig. 2). This kind of perturbation can represent, e.g., the effects of longitudinal slips of the robot's wheels or those of time delays present in the control-input channels. In this case, the output dynamics (10) should be replaced by

$$\dot{\boldsymbol{y}} = \boldsymbol{D}(\theta)[\boldsymbol{u} + \boldsymbol{\mu}], \tag{19}$$

where (by assumption)

$$\forall\, t \geq 0 \ \ \|\boldsymbol{\mu}(t)\| \in [0;\overline{m}], \quad 0 < \overline{m} < \infty. \tag{20}$$

Now, the positional error dynamics take the form

$$\begin{aligned}\dot{F} &= \nabla \boldsymbol{F}^\top \dot{\boldsymbol{y}} \overset{(19)}{=} \nabla \boldsymbol{F}^\top \boldsymbol{D}(\theta)\,[\boldsymbol{u} + \boldsymbol{\mu}] \\ &\overset{(11)}{=} s\nabla \boldsymbol{F}^\top \boldsymbol{w} + \nabla \boldsymbol{F}^\top \boldsymbol{D}(\theta)\boldsymbol{\mu} \\ &\overset{(13)}{=} s\nabla \boldsymbol{F}^\top k_p \left[\lfloor F\rceil^{1+\delta} + \lfloor F\rceil^{1-\delta}\right]\vartheta + \nabla \boldsymbol{F}^\top \boldsymbol{D}(\theta)\boldsymbol{\mu} \\ &= -sk_p \,\mathrm{sign}\,(F)\,\|\nabla \boldsymbol{F}\| \left[|F|^{1+\delta} + |F|^{1-\delta}\right] \\ &\quad + \nabla \boldsymbol{F}^\top \boldsymbol{D}(\theta)\boldsymbol{\mu}. \end{aligned} \tag{21}$$

Let us consider again the positive definite function $V(F) \triangleq F^2$. Its time derivative $\dot{V}(F) = 2F\dot{F}$ along the solutions of (21) can be assessed as follows:

$$\begin{aligned}\dot{V} &\overset{(21)}{=} -2sk_p \,\|\nabla \boldsymbol{F}\| \left[|F|^{2+\delta} + |F|^{2-\delta}\right] \\ &\quad + 2F\nabla \boldsymbol{F}^\top \boldsymbol{D}(\theta)\boldsymbol{\mu} \\ &\leq -2sk_p \,\|\nabla \boldsymbol{F}\| \left[|F|^{2+\delta} + |F|^{2-\delta}\right] \\ &\quad + 2\,|F|\,\|\nabla \boldsymbol{F}\|\,\|\boldsymbol{D}(\theta)\|\,\overline{m} \\ &\leq -2k_p\underline{s}\,|F|\,\|\nabla \boldsymbol{F}\| \left[|F|^{1+\delta} + |F|^{1-\delta}\right] \\ &\quad + 2\,|F|\,\|\nabla \boldsymbol{F}\|\,\overline{m}\sqrt{1+L_Z^2} \\ &\leq -2gk_p\underline{s}\,|F| \cdot \left[|F|^{1+\delta} + |F|^{1-\delta} - \frac{\overline{m}\sqrt{1+L_Z^2}}{k_p\underline{s}}\right] \\ &= -2gk_p\underline{s}\,|F| \cdot r(F,\overline{m}), \end{aligned} \tag{22}$$

where we used (8) from the assumption A2, $\underline{s} = \inf_{t\geq 0} s(t) > 0$, while $\|\boldsymbol{D}(\theta)\| \leq \sqrt{1+L_Z^2}$ results from a well-known relationship between the induced 2-norm and the Frobenius norm of a matrix (cf. Skogestadt and Postlethwaite, 2005). Upon (22) one concludes that $\dot{V} \leq 0$ if $r(F,\overline{m}) > 0$, which leads to the following (conservative) robustness condition:

$$|F|^{1+\delta} + |F|^{1-\delta} > \frac{\overline{m}\sqrt{1+L_Z^2}}{k_p\underline{s}}. \tag{23}$$

If is evident that, for any fixed parameters $k_p > 0$ and $L_Z > 0$, the right-hand side of (23) is a constant, and the smallest value of $|F(\boldsymbol{y})|$ for which the condition (23) is met depends on a selected value of $\delta \in (0;1)$. The plots of function $f(|F|) = |F|^{1+\delta} + |F|^{1-\delta}$ presented in Fig. 3 show that, out of the point for $|F| = 1$, the plots of $f(|F|)$ lie higher for the values of $\delta$ closer to unity. Hence, Fig. 3 illustrates that robustness of the closed-loop dynamics increases when $\delta$ is chosen closer to 1, and that this increase reveals itself more significantly for values of $|F|$ near zero or much larger than one. Moreover, it is evident that the fixed-time controller makes the closed-loop dynamics more robust to perturbation $\boldsymbol{\mu}(t)$ relative to the robustness ensured by an infinite-time controller (the latter corresponds to $\delta = 0$).

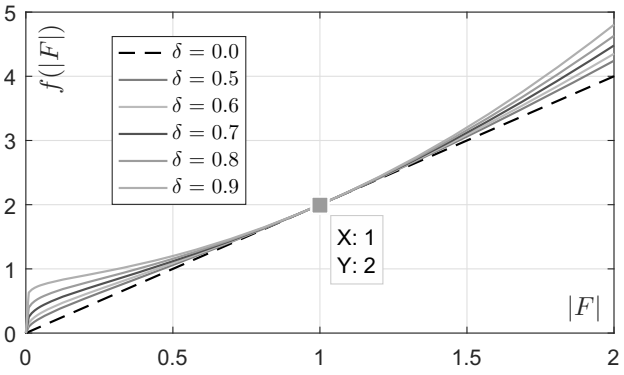



Fig. 3. Plots of function $f(|F|) = |F|^{1+\delta} + |F|^{1-\delta}$ for various values of parameter $\delta$ (together with the limit case for $\delta = 0$, included for better reference); point $(|F|, f(|F|)) = (1, 2)$ is common for all the plots.

Upon the right-hand side of the inequality (23), one can also conclude that robustness to perturbation $\boldsymbol{\mu}(t)$ can be increased by increasing the gain $k_p$ (an intuitive affect) and by decreasing the parameter $L_Z$. However, the latter can be useful up to some extent only, because too short $L_Z$ leads to more intensive amplification of a feedback noise potentially corrupting $\boldsymbol{w}$ in (11), under practical conditions. From the presence of $\underline{s}$ in (23) it is clear that the control inputs constraints compromise robustness as well.

## 5. Simulation verification

In order to verify the proposed fixed-time control system, numerous simulation results were performed using a super-elliptic reference path represented by the set of points satisfying $F(\boldsymbol{y}) \triangleq \sigma(y_1^4 + 16y_2^4 - 1) = 0$ taking $\sigma = 0.1$. The following parameters were used in the simulations: $\alpha = \pi/4\,\text{rad}$, $L_Z = 0.2\,\text{m}$, $\omega_{w\max} = 25\,\text{rad/s}$, $k_p = 1$, $v_d = 0.2\,\text{m/s}$. All the simulations were obtained in the Matlab-Simulink environment using the ode45 solver.

Two sets of results, achieved for 103 stochastically selected initial conditions $\boldsymbol{y}(\boldsymbol{q}(0))$ (denoted by the dots), are presented in Figs. 4 and 5, respectively, for parameters $\delta = 0.1$ and $\delta = 0.7$. The results are complemented by the time-plots of the corresponding (limited) control signals. Since the simulation plots are presented in order to numerically verify the theoretical result formulated in Section 3.2, the positional absolute errors were intentionally computed and presented with a numerical precision which (substantially) exceeds a commonly achievable practical level of errors. Hence, the logarithmic plots of errors in Figs. 4–5 (and also further in Fig. 6) should be analysed and interpreted in the context of Theorem 1.

Analysing the results in Figs. 4–5, one can observe that the value of $\delta$ affects the character of approaching the reference path by point $Z$, which is more smooth for a smaller value of $\delta$ (for smaller $\delta$, the feedback component does not dominate the feedforward component in (13) in a wider vicinity of the path). Moreover, approaching the path in a less smooth manner may cause challenging motion conditions for a real robot when the kinetic effects become more significant. For example, one can observe in Fig. 5 that, during the path-approaching phase with $\delta = 0.7$, the longitudinal speed $u_2(t)$ of the robot quickly decreases close to zero (temporarily even below zero), leading to a very high instantaneous curvature of the robot's motion. In practical applications, this can imply the unwanted slip-skid effects of the wheels and may require forcing the sharp and large-amplitude physical control signals in the robot's actuators.

The upper plots of the absolute positional error shown in Fig. 6 illustrate its fixed-time convergence for the unconstrained case (i.e., for $\omega_{w\max} = \infty$). Note that the upper bound of the settling times becomes smaller for the larger value of parameter $\delta$, which is denoted on the plot by the vertical dashed lines (note: due to a finite numerical accuracy of simulations, the positional error does not reach zero exactly but only a sufficiently small vicinity of zero). On the other hand, the bottom plot in Fig. 6 clearly illustrates that the upper bound of the settling times elongates for the more distant initial conditions, i.e., when the control signals reach their limits during the transient stages (the controller keeps the fixed-time stability but a robot moves slower).

Robustness of the closed-loop system to external control perturbation was verified using two types of external perturbation $\boldsymbol{\mu}(t)$: (1) a piece-wise constant perturbation (called hereafter low-frequency perturbation, LFP) with an amplitude changing pseudo-stochastically (uniformly distributed) every 1 s, and (2) a noise-like perturbation (called hereafter high-frequency perturbation, HFP) with a value changing pseudo-stochastically (uniformly distributed) every sampling time of the simulation. Both perturbations satisfied (20) for $\mu_1, \mu_2 \in [-0.05; 0.05]$, with particular components of $\boldsymbol{\mu} = [\mu_1\ \mu_2]^\top$ interpreted in rad/s and m/s, respectively.

The comparative results shown in Figs. 7 and 8 were obtained for the same initial position of a robot, using four different values of the design parameter $\delta$ to reveal its influence on closed-loop robustness. In order to assess a control cost corresponding to particular cases under study, the norm of the vector $\boldsymbol{u}(t)$ is plotted in Figs. 7 and 8 as well. Additionally, the following quantitative measure was computed:

$$J_u^{[t_1;t_2]} \triangleq \int_{t_1}^{t_2} \|\,\boldsymbol{u}(t)\|^2\,\mathrm{d}t, \qquad 0 \le t_1 < t_2, \tag{24}$$

which represents here the cost of a control process within

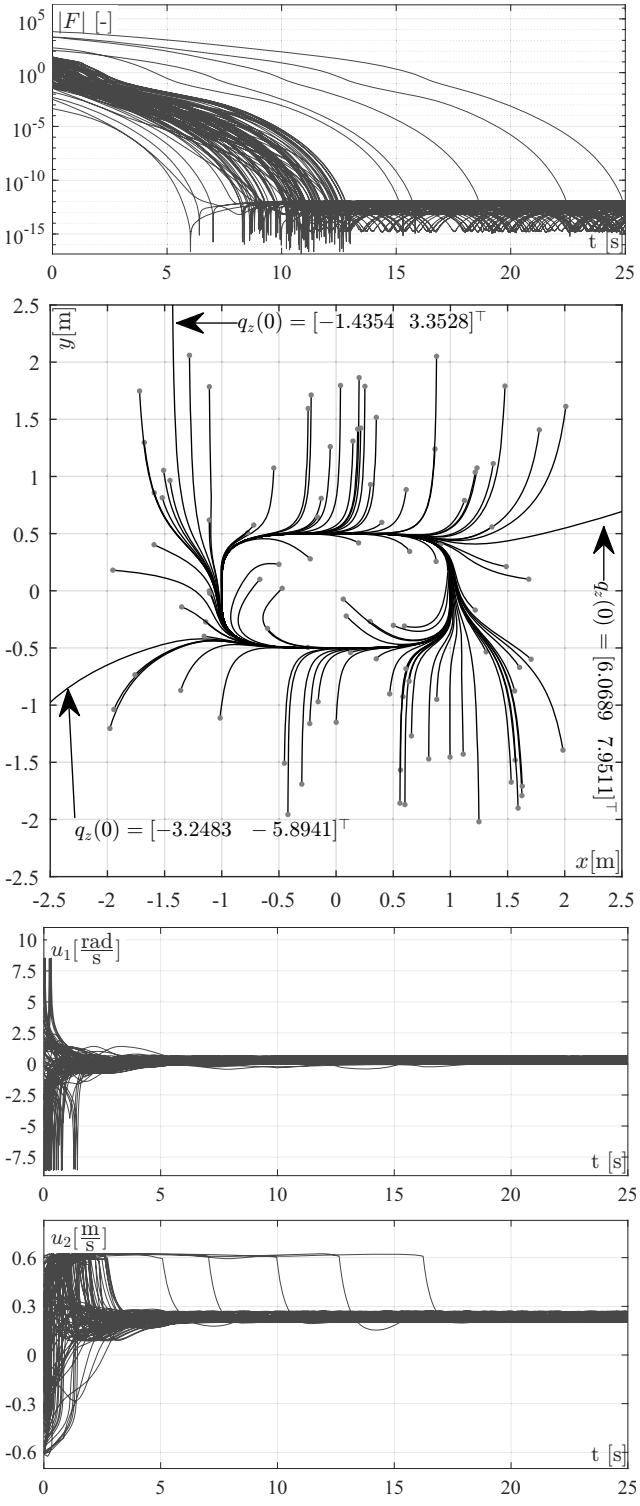



Fig. 4. Time evolution of positional absolute errors and a set of paths drawn by the robot's point $Z$ when starting from various initial conditions (close to and far from the reference path), complemented with the corresponding time plots of control signals: the case for $\delta = 0.1$.

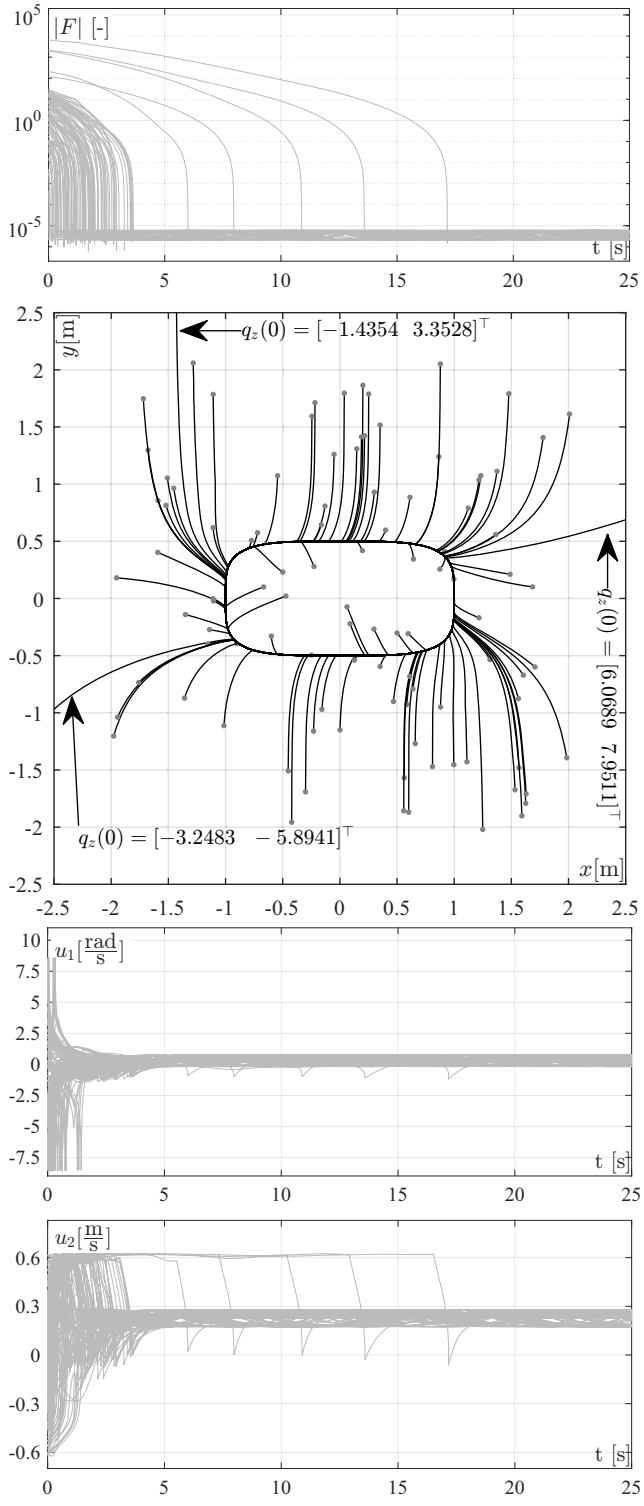



Fig. 5. Time evolution of positional absolute errors and a set of paths drawn by the robot's point $Z$ when starting from various initial conditions (close to and far from the reference path), complemented with the corresponding time plots of control signals: the case for $\delta = 0.7$.

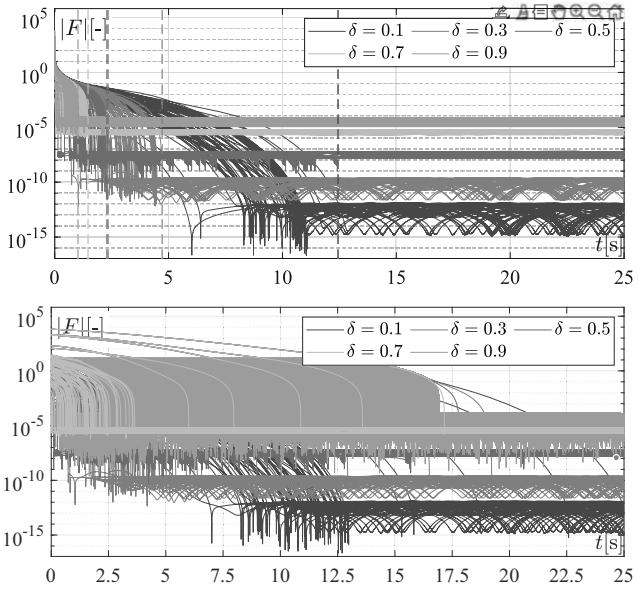



Fig. 6. Absolute positional errors in a logarithmic scale for various values of parameter $\delta$ obtained for a set of 70 randomly selected initial robots configurations in the control-unconstrained case (upper plot) and in the control-constrained case (bottom plot).

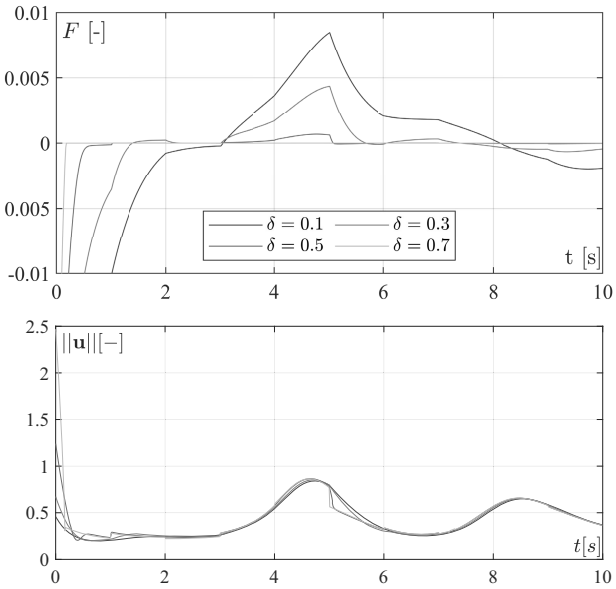



Fig. 7. Time-plots of positional errors in a linear scale (upper plot) and the corresponding plot of a control-vector norm illustrating an increase in closed-loop robustness to external low-frequency perturbation (LFP) $\boldsymbol{\mu}(t)$ by selecting a larger value of parameter $\delta$.

Table 1. Values of the control cost (24) obtained in the presence of external perturbation $\boldsymbol{\mu}(t)$ for selected values of design parameter $\delta$ in two cases: with low-frequency perturbation (LFP) and with high-frequency perturbation (HFP).

| | $\delta = 0.1$ | $\delta = 0.3$ | $\delta = 0.5$ | $\delta = 0.7$ | Type |
|---|---|---|---|---|---|
| $J_u^{[0;10]}$ | 2.03 | 2.07 | 2.19 | 2.51 | LFP |
| $J_u^{[1;10]}$ | 1.96 | 1.97 | 1.96 | 1.95 | LFP |
| $J_u^{[0;10]}$ | 1.92 | 1.95 | 2.07 | 2.42 | HFP |
| $J_u^{[1;10]}$ | 1.85 | 1.85 | 1.84 | 1.86 | HFP |

a time horizon $t_2 - t_1$.

The plots of the positional error in Figs. 7–8 indicate that the increase of parameter $\delta$ substantially improves robustness of a closed-loop system to both types of perturbation.

The plots of the control vector norm in Figs. 7–8 reveal that, after the vanishing of the transient stage, an increase in robustness does not require any substantial increase of the control cost. The numerical values presented in Table 1 confirm this claim, with the values of the control cost $J_u^{[1;10]}$ almost the same for all the selections of parameter $\delta$. A slight increase in the cost $J_u^{[0;10]}$ visible in Table 1 comes from the transient performance, which makes the robot (as expected) move point $Z$ more rapidly toward the path for larger $\delta$.

## 6. Experimental results

The proposed fixed-time control system was validated in a fast-prototyping laboratory setup illustrated by a block scheme in Fig. 9. The MTracker robot (a differentially-driven mobile platform designed and built in the Institute of Automatic Control and Robotics of Poznan University of Technology (PUT); see Fig. 10) used in the experiments was equipped with a radio link to provide on-line communication with an external PC equipped with the Matlab software, where most of the functional control blocks were implemented. During the control process, a resultant control vector $\boldsymbol{u}$ was transformed to the instantaneous desired speeds for the wheels $\boldsymbol{\Omega}_d = \boldsymbol{J}^{-1}\boldsymbol{u}$, which next were sent to the robot trough a radio link as reference inputs to the two independent speed controllers implemented on-board. The main feedback from the robot's configuration was possible thanks to the odometry calculations. Kinematic parameters of the MTracker include a wheel radius $r = 0.025\,\mathrm{m}$ and a distance between the wheels $2b = 0.145\,\mathrm{m}$ (cf. Fig. 1).

The experimental tests were conducted for the same reference path as used for the simulation purposes and with the same geometric location of point $Z$ (i.e., $L_Z = 0.2\,\mathrm{m}$, $\alpha = \pi/4\,\mathrm{rad}$). The following parameters were selected for the controller: $k_p = 1.0$, $v_d = 0.1\,\mathrm{m/s}$, $\omega_{w\,\max} = 25\,\mathrm{rad/s}$. In the fast-prototyping system, all the signals were updated in the control system with an average

sampling frequency $f_p \approx 31$ Hz.

Figure 11 presents the comparative experimental results illustrating time evolutions of the positional absolute errors and a set of paths drawn by MTracker's point $Z$ for various initial positions. For every initial condition, three independent trials were conducted with different values of parameter $\delta$. One can observe that in all the cases the movement of point $Z$ is relatively smooth, and the convergence is faster for a larger value of $\delta$. Additionally, one can see an improvement in the control accuracy for $\delta = 0.2$ (in most duration of the experiments), relative to the case with $\delta = 0.1$. However, for $\delta = 0.3$, any further reliable improvement is not evident from the results (a slight improvement of accuracy is visible only temporarily), while the additional medium-frequency oscillations occur in the control signals. The latter effects are probably a consequence of the sampling process of signals in the fast prototyping system, which is not of high enough frequency in the case of a larger value of $\delta$ (the larger $\delta$, the more rapid changes of control signals can be required for a non-Lipschitz part of the controller).

Comparative results presented in Fig. 12 (obtained for the same initial position of point $Z$) reveal a change in closed-loop robustness with selection of positive values of $\delta$ relative to the case of $\delta = 0$ which corresponds to the infinite-time version of the path-following controller (cf. (13)–(14)). Analysing the results, it can be observed that also in practical conditions the fixed-time controller can be more robust than its infinite-time version, at least in the sense of the measure $\limsup_{t>t^*} |F(t)|$, where $t^*$ is a sufficiently long duration of a robot movement.

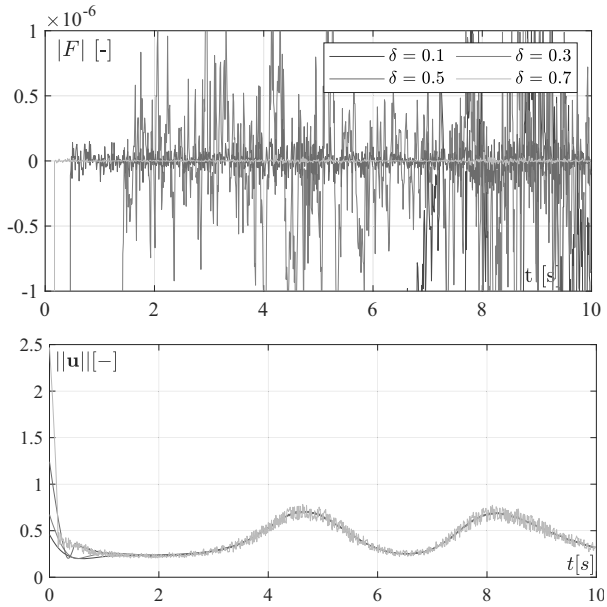



Fig. 8. Time-plots of positional errors in a linear scale (upper plot) and the corresponding plot of a control-vector norm illustrating an increase in closed-loop robustness to external high-frequency perturbation (HFP) $\boldsymbol{\mu}(t)$ by selecting a larger value of parameter $\delta$.

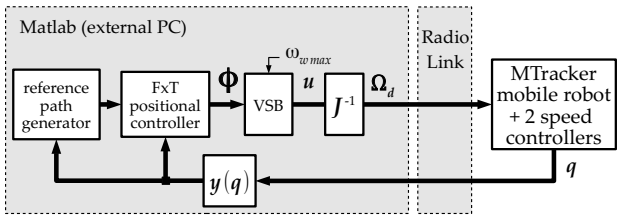



Fig. 9. Block scheme of the experimental control system with the MTracker mobile robot implemented in a fast-prototyping setup.

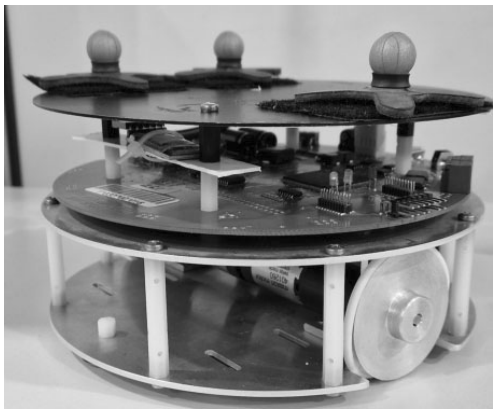


Fig. 10. Experimental laboratory-scale differentially driven robot MTracker built in the Institute of Automatic Control and Robotics of the PUT.

## 7. Conclusions

The fixed-time feedback controller proposed in this paper solves the positional path-following task for unicycle-like kinematics in the presence of control limitations. The presented control method can be useful not only for time-synchronisation of a multi-robot system, but also to increase closed-loop robustness to perturbations corrupting a control channel (i.e., speed components of a robot). Assessment of an upper bound of the convergence time is possible (see, e.g., Sanchez-Torres *et al.*, 2020); however, it is usually (very) conservative due to the inequalities used in the stability analysis and taking into account the worst case scenario of the input signals saturation process (Sobański *et al.*, 2025). When implementing the fixed-time control system in a discrete-time domain, one has to pay attention to the sampling frequency, which should be high enough for larger values of parameter $\delta$ in order to keep robustness on an expected level and avoid oscillatory evolution of control signals. Application of the fixed-time control law may be extended in the future to car-like kinematics by

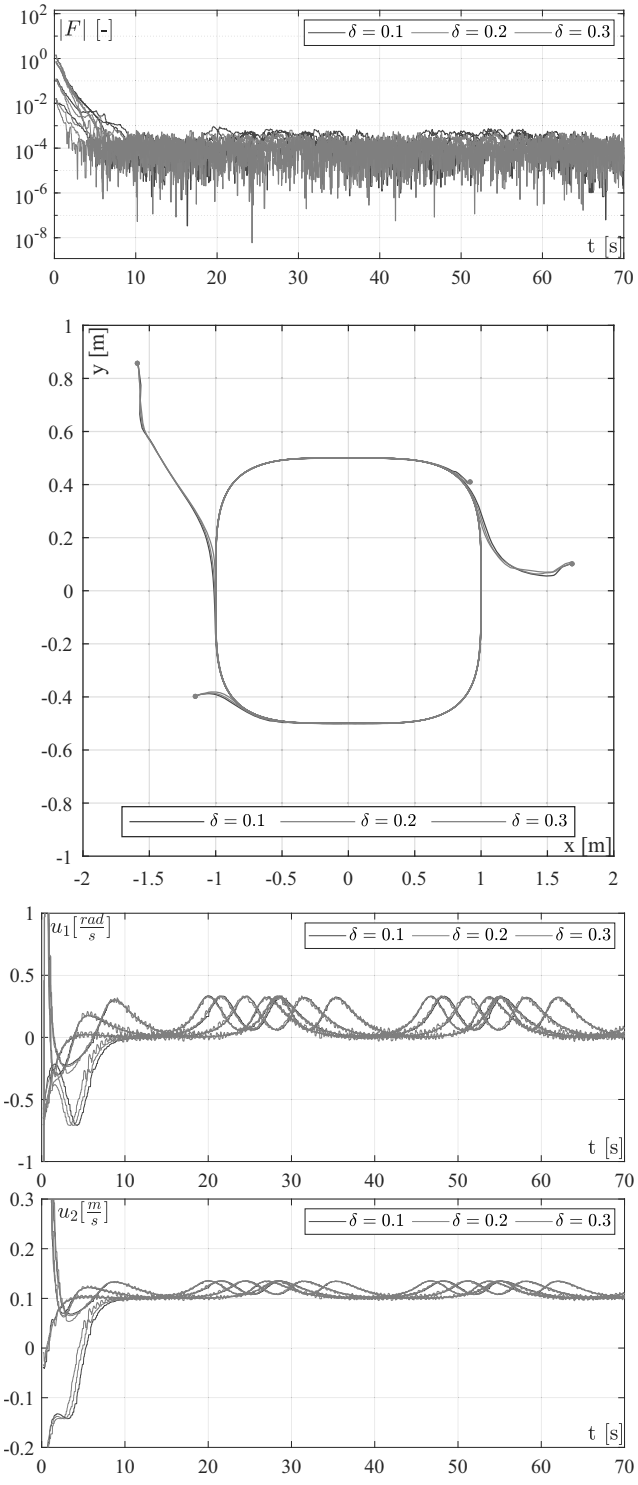



Fig. 11. Collection of comparative experimental results illustrating time evolutions of positional absolute errors and a set of paths drawn by MTracker's point $Z$ when starting from four different initial conditions (denoted by the dots in the XY plot), complemented with the corresponding time plots of control signals for three selected values of parameter $\delta$.

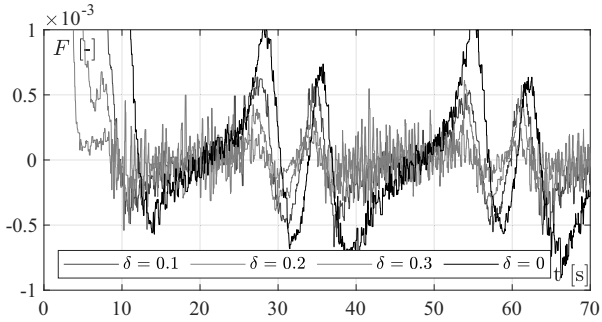



Fig. 12. Comparative experimental results of positional error evolution illustrating an increase in closed-loop robustness achievable for larger values of parameter $\delta$ relative to the case of *infinitely convergent* control version corresponding to $\delta = 0$.

using the control framework introduced by Michałek and Kozłowski (2012).

## Acknowledgment

The authors thank Rafał Sobański for his help in the commissioning of the experimental setup. This work was supported by the statutory fund no. 0211/SBAD/0125 of the Institute of Automatic Control and Robotics, Poznan University of Technology.

## References

Aldana-Lopez, R., Gomez-Gutierrez, D., Jimenez-Rodriguez, E., Sanchez-Torres, J.D. and Defoort, M. (2019). Enhancing the settling time estimation of a class of fixed-time stable systems, *International Journal of Robust Nonlinear Control* **29**(12): 4135–4148.

Bhat, S.P. and Bernstein, D.S. (2000). Finite-time stability of continuous autonomous systems, *SIAM Journal on Control and Optimization* **38**(3): 751–766.

Consolini, L., Maggiore, M., Nielsen, C. and Tosques, M. (2010). Path following for the PVTOL aircraft, *Automatica* **46**(8): 1284–1296.

Dai, S.-L., Lu, K. and Jin, X. (2021). Fixed-time formation control of unicycle-type mobile robots with visibility and performance constraints, *IEEE Transactions on Industrial Electronics* **68**(12): 12615–12625.

de Wit, C.C., Siciliano, B. and Bastin, G. (1996). *Theory of Robot Control*, Springer-Verlag, New York.

Efimov, D. and Polyakov, A. (2021). Finite-time stability tools for control and estimation, *Foundations and Trends in Systems and Control* **9**(2–3): 1–212.

Gao, F., Huang, J., Wu, Y. and Zhao, X. (2022). A time-scale transformation approach to prescribed-time stabilisation of non-holonomic systems with inputs quantisation, *International Journal of System Science* **53**(8): 1796–1808.

Garg, K., Arabi, E. and Panagou, D. (2022). Fixed-time control under spatiotemporal and input constraints: A quadratic programming based approach, *Automatica* **141**(110314): 1–9.

Lapierre, L., Soetanto, D. and Pascoal, A. (2006). Nonsingular path following control of a unicycle in the presence of parametric modelling uncertainties, *International Journal of Robust Nonlinear Control* **16**(10): 485–503.

Lin, L., Wu, P., He, B., Chen, Y., Zheng, J. and Peng, X. (2021). The sliding mode control approach design for nonholonomic mobile robots based on non-negative piecewise predefined-time control law, *IET Control Theory & Applications* **15**(9): 1286–1296.

Mazur, A. and Dyba, F. (2025). A robust path following algorithm based on the orthogonal bishop parametrization for a non-holonomic mobile manipulator, *International Journal of Applied Mathematics and Computer Science* **35**(2): 209–224, DOI: 10.61822/amcs-2025-0015.

Mazur, A. and Szakiel, D. (2009). On path following control of non-holonomic mobile manipulators, *International Journal of Applied Mathematics and Computer Science* **19**(4): 561–574, DOI: 10.2478/v10006-009-0044-0.

Michałek, M. and Kozłowski, K. (2012). Feedback control framework for car-like robots using the unicycle controllers, *Robotica* **30**(4): 517–535.

Michałek, M.M. and Gawron, T. (2018). VFO path following control with guarantees of positionally constrained transients for unicycle-like robots with constrained control input, *Journal of Intelligent & Robotic Systems* **89**(1–2): 191–210.

Michałek, M.M., Przybylski, M.J. and Sobański, R.M. (2025). Fixed-time controller for a unicycle in the positional path-following task, *in* A. Mazur and C. Zieliński (Eds), *Advances of Robotics*, Wrocław University of Science Technology Press, Wrocław, pp. 75–84, (in Polish)

Morin, P. and Samson, C. (2008). Motion control of wheeled mobile robots, *in* B. Siciliano and O. Khatib (Eds), *Springer Handbook of Robotics*, Springer, Cham, pp. 799–826.

Morro, A., Sgorbissa, A. and Zaccaria, R. (2011). Path following for unicycle robots with arbitrary path curvature, *IEEE Transactions on Robotics* **27**(5): 1016–1023.

Moulay, E. and Perruquetti, W. (2006). Finite-time stability and stabilization: State of the art, *in* C. Edwards *et al.* (Eds), *Advances in Variable Structure*, Springer-Verlag, Berlin/Heidelberg, pp. 23–41.

Oriolo, G., Luca, A.D. and Vendittelli, M. (2002). WMR control via dynamic feedback linearization: Design, implementation, and experimental validation, *IEEE Transactions on Control Systems Technology* **10**(6): 835–852.

Ou, M., Sun, H., Zhang, Z. and Gu, S. (2022). Fixed-time trajectory tracking control for nonholonomic mobile robot based on visual servoing, *Nonlinear Dynamics* **108**: 251–263.

Parsegov, S., Polyakov, A. and Shcherbakov, P. (2012). Nonlinear fixed-time control protocol for uniform allocation of agents on a segment, *2012 IEEE 51st IEEE Conference on Decision and Control (CDC), Maui, USA*, pp. 7732–7737.

Płaskonka, J. (2015). Different kinematic path following controllers for a wheeled mobile robot of (2,0) type, *Journal of Intelligent & Robotic Systems* **77**: 481–498.

Polyakov, A. (2012). Nonlinear feedback design for fixed-time stabilization of linear control systems, *IEEE Transactions on Automatic Control* **57**(8): 2106–2110.

Sanchez-Torres, J.D., Defoort, M. and Munoz-Vazquez, A.J. (2020). Predefined-time stabilisation of a class of nonholonomic systems, *International Journal of Control* **93**(12): 2941–2948.

Skogestadt, S. and Postlethwaite, I. (2005). *Multivariable Feedback Control: Analysis and Design, 2nd Edn*, John Wiley & Sons, Hoboken.

Sobański, R., Michałek, M.M. and Defoort, M. (2025). Fixed-time VFO control design for nonholonomic mobile robots with constrained control inputs, *IEEE Transactions on Cybernetics* **55**(7): 3038–3050.

Yao, W., de Marina, H.G., Lin, B. and Cao, M. (2021). Singularity-free guiding vector field for robot navigation, *IEEE Transactions on Robotics* **37**(4): 1206–1221.

Yao, W., Lina, B., Anderson, B.D.O. and Cao, M. (2023). Topological analysis of vector-field guided path following on manifolds, *IEEE Transactions on Automatic Control* **68**(3): 1353–1368.

Zhang, J., Yu, S. and Yan, Y. (2019). Fixed-time output feedback trajectory tracking control of marine surface vessels subject to unknown external disturbances and uncertainties, *ISA Transactions* **93**: 145–155.

Zhou, S., Wei, Y., He, W. and Cao, J. (2025). Prescribed-time stabilization for uncertain Euler–Lagrangian systems: A cascade and singularity-free design, *2025 IEEE International Conference on Systems, Man, and Cybernetics (SMC), Vienna, Austria,* pp. 5705–5710.



**Maciej Marcin Michałek** received his PhD and DSc (habilitation) degrees in the field of automatic control and robotics from the Poznan University of Technology (PUT), Poland, in 2006 and 2015, respectively. He currently works as a full professor in the Institute of Automatic Control and Robotics there. His present research interests include modelling and control design for dynamical systems, especially for nonholonomic mobile robots, N-trailer structures, and intelligent/automated vehicles. He was an editorial board member of the *Journal of Intelligent & Robotic Systems* (2011–2023) and the *Journal of the Franklin Institute* (2020–2022) as well as a conference editorial board member for the IEEE Control Systems Society (2017–2025), and he currently serves as an associate editor for *IEEE Transactions on Cybernetics* and *IEEE Transactions on Aerospace and Electronic Systems*.



**Mikołaj Jerzy Przybylski** received his MSc degree in automatic control and robotics from the Poznan University of Technology (PUT), Poland, in 2025. He is currently an assistant lecturer with the Institute of Automatic Control and Robotics, PUT. His research interests include control design for mobile robots and articulated vehicles.

Received: 29 November 2025
Revised: 23 February 2026
Accepted: 24 April 2026